Talanta 117 (2013) 536–542

Contents lists available at ScienceDirect

Talanta

journal homepage: www.elsevier.com/locate/talanta

Biocompatible phosphonic acid-functionalized silica nanoparticles for sensitive detection of hypoxanthine in real samples

Min Liu [a], Shanshan Chen [a], Xianzheng Zhao [a], Yuhang Ye [a], Juan Li [a], Qinshu Zhu [a], Bo Zhao [a], Wenbo Zhao [a,*], Xiaohua Huang [a,*], Jian Shen [a,b]

[a] Jiangsu Key Laboratory of Biofunctional Materials, College of Chemistry and Materials Science, Nanjing Normal University, Nanjing 210023, PR China
[b] Research Center of Surface and Interface Chemistry and Engineering Technology, School of Chemistry and Chemical Engineering, Nanjing University, Nanjing 210093, PR China

ARTICLE INFO

Article history:
Received 21 May 2013
Received in revised form
28 August 2013
Accepted 31 August 2013
Available online 7 September 2013

Keywords:
Silica
Phosphonic acid-functionalized
Biomimetic
Xanthine oxidase
Biosensor

ABSTRACT

A novel hypoxanthine biosensor fabricated by immobilizing the xanthine oxidase (XOD) onto the phosphonic acid-functionalized silica (SiO_2-P) film on the surface of glassy carbon electrode (GCE) was designed and constructed in this work. A biomimetic platform was designed with the phosphonic acid-functionalized silica nanoparticles (SiO_2-P NPs) synthesized by the method of reverse microemulsion and electrostatic binding. In such a platform, XOD was selected as model protein to fabricate hypoxanthine biosensor based on SiO_2-P NPs. The nanocomposite was characterized with transmission electron microscopy (TEM), energy dispersive X-ray spectrometer (EDS) and electrochemical impedance spectroscopy (EIS). Based on the advantageous functions of SiO_2-P NPs, the entrapped XOD could preserve its bioactivity and exhibited an excellent electrochemical behavior with a formal potential of −0.37 V in phosphate buffer solution (PBS, pH=7). Response studies to hypoxanthine were carried out using current–time response curve. The biosensor exhibited a wide linear response ranging from 1.00×10^{-6} to 2.61×10^{-4} M. The detection limit of 2.33×10^{-7} M at a signal-to-noise ratio of 3 was lower than that most reported previously. In addition, the electrode modified with XOD/(SiO_2-P NPs) film also had a strong anti-interference ability in the presence of uric acid (UA) and ascorbic acid (AA). The assay results of hypoxanthine in fish samples were in a good agreement with the reference values.

1. Introduction

The development of nanomaterials for the ultra sensitive detection of biological species has received great attention because of their unique optical, electronic, chemical and mechanical properties [1–5]. Analysts in this field are always enthusiastic about finding new nanomaterials with good biocompatibility to improve the behavior of biosensors [6,7]. Central to tackling this issue is surface functionalization of nanomaterials and elucidating the interfaces and interactions between nanomaterials and biological species [8].

Recently, modified silica materials have been extensively studied because they can provide a suitable microenvironment for biomolecule immobilization, and have been widely applied in the detection of proteins, antigen–antibody and cells [9,10]. Hence, to enhance the biocompatibility of silica-based materials is a crucial point for the development of electrochemical biosensor. Much attention has been paid to the synthesis SiO_2 composite materials and used these biocompatible materials to make biosensors, for example, Fe_3O_4@a–SiO_2@hemin [11], Hb–Au NPs–C@SiO_2/GCE [12] and polymer SiO_2 NPs for immobilization of proteins on electrode surface can solve the toxicity problems of materials.

Phosphonic acid-functionalized materials had been applied in various fields such as bioelectrochemistry, electroanalysis and biomimetic membranes. Phosphonate radical is negative with the same charge repelled, therefore phosphonic acid-functionalized materials possess perfect dispersity, and can also improve the conductivity of original materials. Moreover, P=O bond and phospholipids construct the main components of the bilayer in cellular membranes [13,14]. So adding the P=O bond (phosphonate group) into biomaterials can be viewed as bionic building to improve the biocompatibility of conventional materials. In this work, phosphonate-terminated silica nanoparticles (SiO_2-P NPs) were obtained using water-in-oil (W/O) micro-emulsion. The biocompatibility of SiO_2-P NPs was investigated. Further, a novel hypoxanthine biosensor fabricated by immobilizing the xanthine oxidase (XOD) onto the phosphonic acid-functionalized silica (SiO_2-P) film on the surface of glassy carbon electrode (GCE) was designed. XOD, which participates in

* Corresponding authors. Tel.: +86 25 85891536; fax: +86 25 83598280.
E-mail addresses: zhaowenbo@njnu.edu.cn (W. Zhao), xiaohuahuang_njnu@yahoo.cn (X. Huang).

0039-9140/$ - see front matter © 2013 Elsevier B.V. All rights reserved.
http://dx.doi.org/10.1016/j.talanta.2013.08.061

many important biochemical reactions, is a key enzyme in purine metabolism [15]. It has attracted a lot of attention because of its potential role in tissue and vascular injuries, and in inflammatory diseases and chronic heart failure [16,17]. It catalyzes the oxidation of hypoxanthine to xanthine and that of xanthine to uric acid with concomitant reduction of molecular oxygen [18]. The determination of hypoxanthine is of a considerable indicator for the quality control of fish products in food industries as well. Therefore, it is significant to develop a quick and effective detection method for the determination of hypoxanthine [18,19]. More details about the hypoxanthine biosensor based on SiO_2-P NPs we prepared were presented.

2. Experiments

2.1. Reagents

Bovine milk xanthine oxidase (XOD, Sigma-Aldrich, USA) was used as received, Triton X-100 was purchased from Aladdin Chemistry Co. Ltd. (China). Tetraethyl silicate (TEOS), hexanol and absolute ethyl alcohol were obtained from Sinopharm Chemical Reagent Co. Ltd (China). Aqueous ammonia solution (NH_4OH, 71 wt% water, 29 wt% ammonia) was obtained from Shanghai Lingfeng Chemical Co. Ltd. (China) and cyclohexane was obtained from Shanghai Shengbo Chemical Co. Ltd. (China). Organosilanes 3-(trihydroxysilyl)-propylmethylphosphonate (THPMP) was purchased from GELEST Inc. (USA). All the above reagents were used without further purification. Phosphate buffer solution (PBS, 0.1 M) was prepared by mixing stock standard solution of Na_2HPO_4 and NaH_2PO_4. All other chemicals were of analytical grade and all solutions prepared with double-distilled water.

2.2. Preparation of SiO_2-P nanopariticles

SiO_2 NPs were synthesized using reverse microemulsion method, the preparation process of SiO_2-P NPs (Scheme 1) was described in the reference [20]. Firstly, 1.926 g Triton X-100, 1.6 mL hexanol, 480 μL water and 100 μL of aqueous ammonia were added into 7.5 mL cyclohexane and stirred for 30 min at room temperature, and then 100 μL of TEOS was added. Aqueous ammonia served as both reactant (H_2O) and catalyst (NH_3) for the hydrolysis of TEOS. The mixture was allowed to stir for 24 h, followed by the addition of THPMP for particle surface modification. The mixture was further reacted for another 24 h, and the SiO_2 NPs were released from the microemulsion by the addition of ethanol. The particles were separated from the reaction mixture by centrifugation at 4000 rpm for 10 min and washed three times with ethanol and double-distilled water respectively. The as-prepared SiO_2-P NPs were stable at room temperature even after 6 months storage.

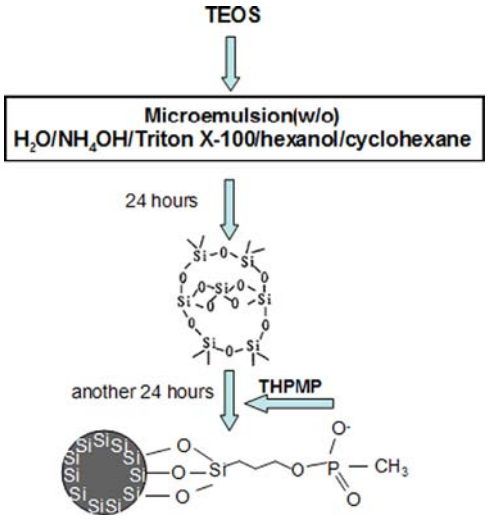

Scheme 1. Schematic representation of preparation SiO_2-P NPs.

2.3. Construction of the XOD/(SiO_2-P NPs)/GCE modified electrode

The glassy carbon electrode was polished with 0.3 and 0.05 μm alumina slurry, and then sonicated in ethanol and double-distilled water for 5 min each. After that, the GCE was allowed to dry at room temperature to form a mirror-like surface. To prepare the modified electrode, firstly, 8.0 μL of the obtained SiO_2-P NPs solution was dropped onto the electrode surface and dried in air. Then, 8.0 μL of XOD solution in PBS (pH=7.0) was dropped onto the surface of (SiO_2-P NPs)/GCE and kept overnight at 4 °C. Finally the XOD/(SiO_2-P NPs)/GCE was obtained. The other electrodes used as contrast samples were prepared by the same modified method. When not in use, the electrodes were stored at 4 °C in a refrigerator.

2.4. Calculator simulation method

Crystal structure of XOD used for starting configuration in the simulation was extracted from the Protein Data Bank identifier 1FIQ. The 3D structure of XOD was generated in Discovery Studio 2.1 (Accelrys, USA) [21].

The molecular structure of methyl phosphonate was depicted. It also was fully optimized at the B3LYP (DFT) level with the 6–31+G^* basis set and characterized by the calculations of vibrational frequencies at the same level. All these theoretical calculations were carried out using GAUSSIAN 03 suite of programs [22] and using the default convergence criteria.

2.5. Apparatus and measurements

Transmission electron microscopy (TEM) images were obtained using an interface high-resolution transmission electron microscopy (HITACHI H-7650, Japan). Element content was analyzed by using of an energy dispersive X-ray spectrometer (EDS, JSM-5610LV/NORAN-VANTAGE). Circular dichroism spectra (CD) in the far-UV (with the range from 190 to 250 nm) were measured on a JASCO J-715 spectropolarimeter using a 0.1 cm quartz cuvette. The contents of α-helix, β-sheet, β-turn and the random coil conformation were calculated using the JASCO710 program. UV–vis spectra were recorded on a Cary 5000 UV–vis-NIR spectrometer (Varian). The concentration of XOD is the same as that in each XOD/SiO_2 and XOD/SiO_2-P system. All electrochemical experiments were performed on a CHI760C electrochemical analyzer (CH Instruments, Inc., US), using a conventional three-electrode system with an glassy carbon electrode (GCE, 3 mm in diameter, Shanghai Chenhua, China) as the working electrode, a platinum wire as the auxiliary electrode and a saturated calomel electrode (SCE) as the reference electrode. Cyclic voltammogram (CV) experiments were carried out in quiescent solution at 100 mV s^{-1} in 5 mL of 0.1 M PBS, and the solution was purged with high purity nitrogen prior to and blanked with during the electrochemical experiments. Electrochemical impedance measurements were performed in a 0.1 M KCl containing 5 mM $Fe(CN)_6^{3-/4-}$ (1:1) and plotted in the form of complex plane diagrams (Nyquist plots). The current–time curves were recorded in a stirred cell with a successive addition of hypoxanthine standard solution to the cell.

2.6. Determination of hypoxanthine for fish freshness

A piece of fish meat (4–5 g) from crucian carp fillet was homogenized in 15 mL water at room temperature and the solution was then filtered through a filter membrane (0.2 μm pore size). Ultra-pure water was then added into the filtrate producing a total volume of 50 mL homogenized sample solution. A mixture containing equal volumes of the fish extract and 0.1 M PBS was performed for fish freshness analysis. All sample solutions were prepared immediately for each experiment. This was adapted for potentiometric biosensing of hypoxanthine.

3. Results and discussion

3.1. Characterization of morphology, biocompatibility and electrochemical impedance of the SiO_2-P nanoparticles

Transmission electron microscopy (TEM) analysis is essential to examine the detailed microstructures of these nanoparticles. TEM images of SiO_2 and SiO_2-P presented in Fig. 1 showed that SiO_2 NPs were assuredly agglomerated (Fig. 1a) while SiO_2-P NPs were consisted of extremely monodispersed circular nanoparticles (Fig. 1b) with the average diameter of 50 nm. The size of SiO_2 NPs which modified with phosphonate group did not change obviously compared with simple SiO_2 NPs.

Energy dispersive X-ray spectrometer (EDS) measurements of the SiO_2-P structure revealed that it consisted of 6.96% P, 56.12% O, and 36.92% Si (Fig. 1d). As can be seen from the figures, compared to the SiO_2 NPs (Fig. 1c), there was a clear peak belonged to the P (Fig. 1d), which confirmed the successful combination of SiO_2 NPs and phosphonate group.

Circular dichroism (CD) could be used to probe transitions in the secondary structure of the proteins [23]. Fig. 2A (a–c) showed CD spectra of XOD, XOD after conjugation with 0.33 mg/ml SiO_2-P and 0.33 mg/ml mM SiO_2 in the far-UV region, respectively. CD spectrum took in a cell of 1 mm path length over the wavelength range of 190−250 nm. The positive band at 195 nm and two negative bands at around 208 and 219 nm arised in Fig. 2 were corresponded to the π–π^* transition and n–π^* transition of the amide groups in the XOD peptide chain [24]. Bands of XOD/(SiO_2-P NPs) looked almost the same as pure XOD, only the intensity of the dual bands at 195 nm had a slight increase, indicating that the secondary structure of XOD was not obviously changed.

Secondary structure fractions were calculated using the CD spectra deconvolution program CDNN. The contents of α-helix, antiparallel and β-turn conformation of XOD/(SiO_2-P NPs) increased by 0.6%, 0.4% and 0% while XOD/(SiO_2 NPs) changed 4.3%, 3.9% and 1.0% compared to pure XOD. Due to the small changes mentioned above, the results demonstrated SiO_2-P nanocomposites could essentially maintain the native conformation of XOD. Thus, the secondary structure of XOD was well maintained in the prepared biosensor and SiO_2-P nanocomposites should indeed have good biocompatibility.

The flavin prosthetic group (FAD moiety) is the active center of XOD molecule. The microenvironment changes around the FAD moiety induced by SiO_2 and SiO_2-P reflect the alteration in the

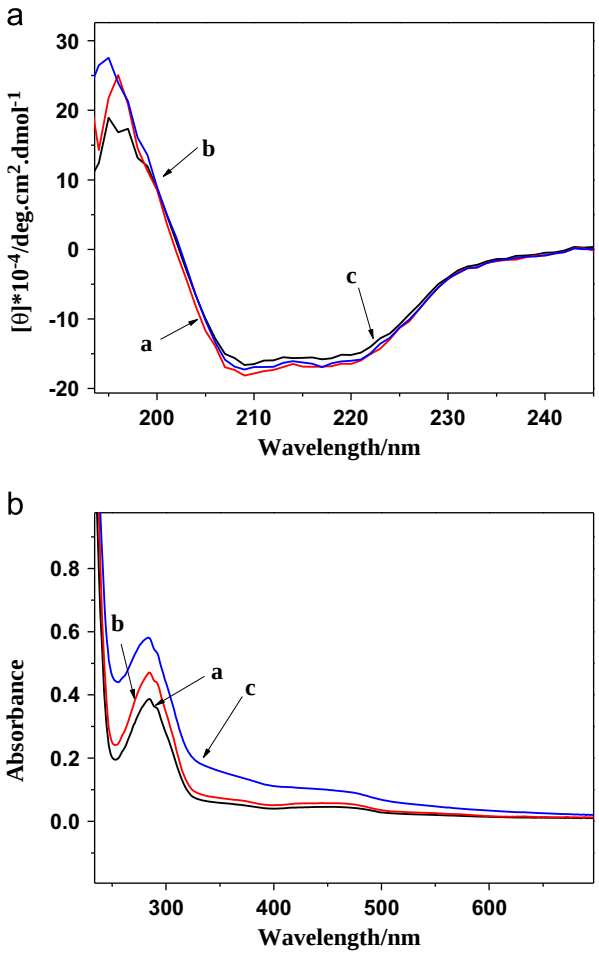

Fig. 2. (A) CD spectra of pure XOD (a), XOD/(SiO_2-P NPs) (b) and XOD/(SiO_2 NPs) (c) in the wavelength region of 190–250 nm. (B) UV–vis absorption spectra of native XOD (a), XOD/(SiO_2-P NPs) (b) and XOD/(SiO_2 NPs) (c).

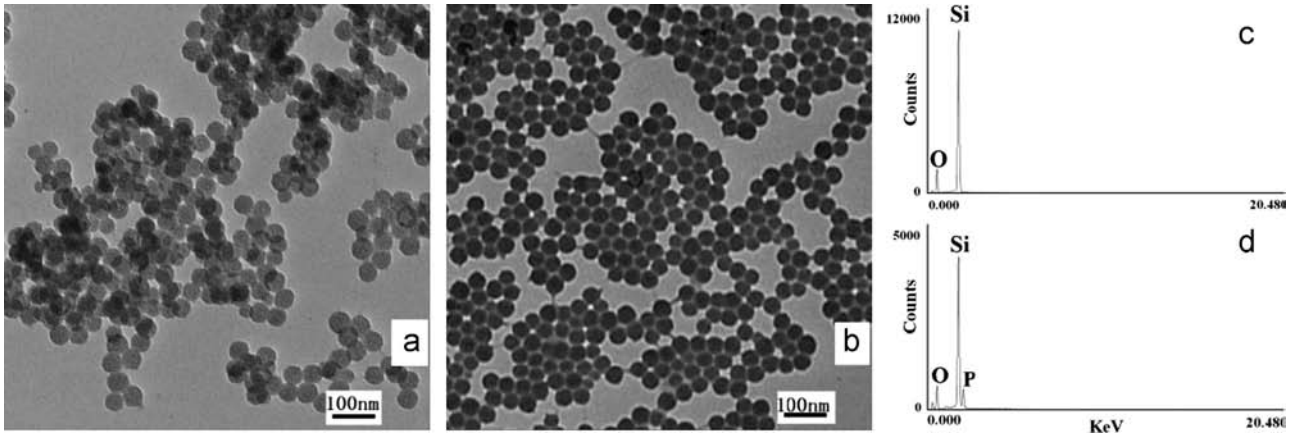

Fig. 1. TEM images of SiO_2 NPs (a) and SiO_2-P NPs (b). Typical EDS spectra taken from SiO_2 NPs (c) and SiO_2-P NPs (d).

conformational structure of the enzyme molecule. This change was studied with UV–vis absorption spectroscopy. The spectrum of the native XOD exhibits two well-defined adsorption bands at approximately 284 and 449 nm (curve a, Fig. 2B), respectively. The band at 284 nm is the characteristic peak of polypeptide chains of the enzyme [25], compared with XOD/(SiO_2-P NPs), addition of SiO_2 into the XOD solution leads to a widen peak and a clear decrease in the intensity of this peak.

The band at 449 nm is the characteristic peak of the FAD moiety [25]. The shape and position of the FAD band can provide information on the environmental influence on the native configuration of XOD, in particular the environments around the FAD moiety. Addition of SiO_2 into the XOD solution (curve c, Fig. 2B) leads to a larger change compared to that of XOD/(SiO_2-P NPs) (curve b, Fig. 2B), the peak becomes flat and dim, but peak of XOD/(SiO_2-P NPs) lookes almost the same as pure XOD, suggesting that the FAD moiety of the enzyme in the presence of SiO_2 becomes less exposed to solvent than that in the presence of SiO_2-P. These results indicate that the interaction of SiO_2-P and XOD can keep the configuration structure of the XOD molecule, in particular the structure around the FAD moiety.

The interaction between of the SiO_2-P NPs and XOD was investigated by calculator simulation. There are two active pockets in XOD named active site1 and active site2. The active site1 involves the main amino acid residues of Met1038, Gly1260 and Gln1040 with a radius of about 5 Å (Fig. 3a and b). The active site2 is FAD active site that made of the amino acid residues of Thr262, Phe337, Asp429, Gly46, Glu45 and Arg426. We specified the approximate center of this active pocket and took several important amino acids that lie within a sphere with the radius of 10 Å. The FAD and important amino acids in the active site were drawn in ball-and-stick in Fig. 4a, and b. From the analysis results we can see that the active pockets of the XOD are much smaller than that of the SiO_2 or SiO_2-P NPs (about 50 nm). That is to say, the active pockets cannot enfold the SiO_2-P NPs and are not big enough for SiO_2-P NPs, and therefore the interactions between them should be interfacial.

On the other hand, in order to investigate the spatial structure of methyl phosphonate we optimized its geometry with the DFT/B3LYP method (Fig. 5). The most remote two points in the methyl phosphonate are H_{15} and H_{10}, which is about 7.94 Å and is the length of the methyl phosphonate molecule to a good approximation. The distances from the surface to the active pockets of the XOD molecule are much bigger than this length and so the methyl phosphonate group can not enter these active pockets and so the

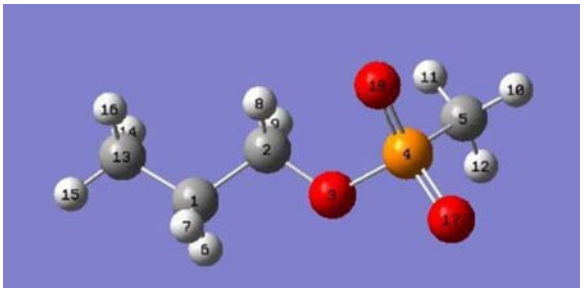

Fig. 5. Molecular structure of methyl phosphonate by DFT studies.

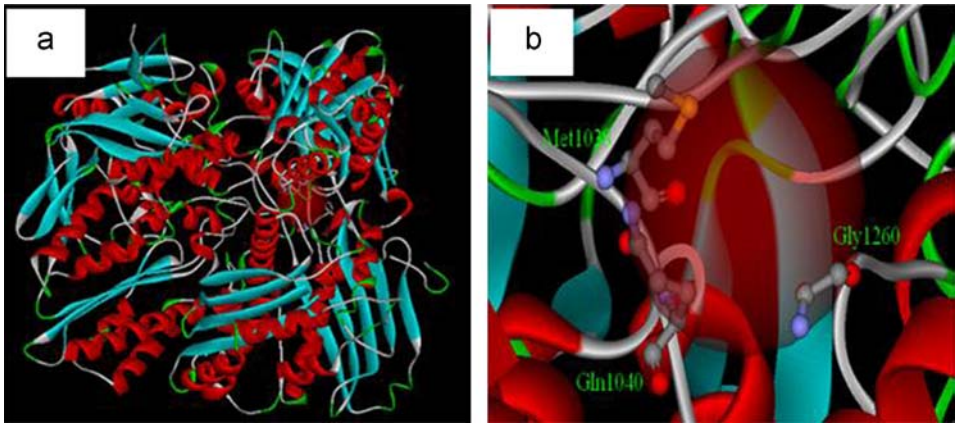

Fig. 3. (a) The active pocket 1 in the whole XOD molecule, and (b) partial enlarged detail.

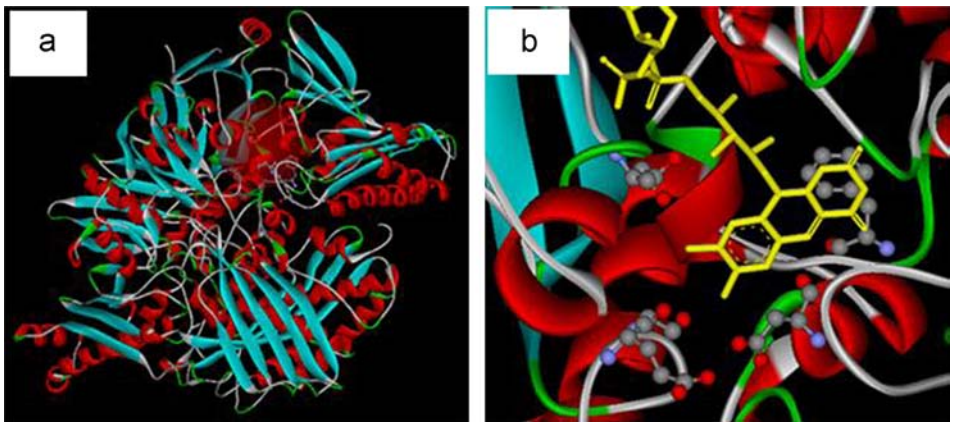

Fig. 4. (a) The active pocket 2 in the whole XOD molecule, and (b) partial enlarged detail.

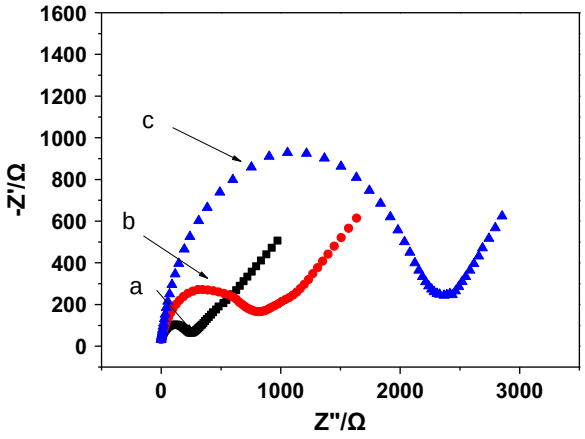

Fig. 6. EIS in 0.1 mM KCl containing 0.5 mM $K_3Fe(CN)_6/K_4Fe(CN)_6$, (a) bare, (b) SiO_2-P modified and (c) SiO_2 modified GCE electrode.

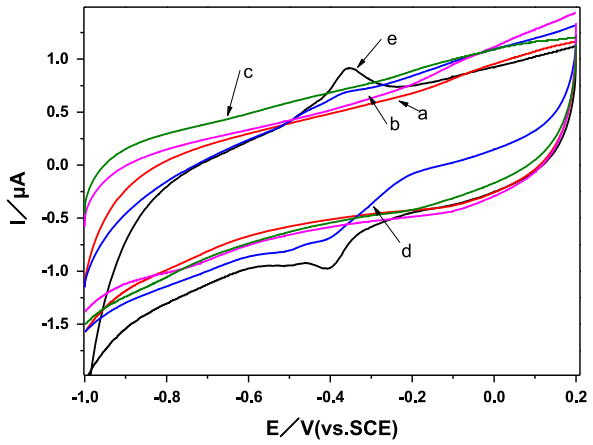

Fig. 7. Cyclic voltammograms of different modified electrodes in 0.1 M PBS (pH=7.0) containing 0.1 M KCl. Bare GCE electrode (a); the (SiO_2 NPs)/GCE electrode (b); the (SiO_2-P NPs)/GCE electrode (c); the XOD/(SiO_2 NPs)/GCE electrode (d) and the XOD/(SiO_2-P NPs)/GCE electrode (e) (scan rate is 100 mV s^{-1}).

SiO_2-P NPs also interfacially contact and then interact with the XOD molecule. This result is in agreement with the above analysis from CD and UV–vis absorption spectra.

The improvement of the conductivity by phosphorylation of SiO_2 NPs can be supported by AC impedance studies. Fig. 6 exhibited the electrochemical impedance spectra of the electrode surface status, shown as Nyquist plot (–Z″ im vs. Z′ re). The Nyquist plot of impedance spectra includes a semicircular portion and a linear portion, with the former at higher frequencies corresponding to the electron-transfer limited process and the latter at lower frequencies corresponding to the diffusion process. The electron transfer resistance (R_{et}) at the electrode surface is equal to the semicircle diameter, which can be used to describe the interface properties of the electrode [26,27]. Fig. 6a showed the electrochemical impedance spectrum of the bare GCE. The semicircle domain was very small, implying a very low electron transfer resistance to the redox-probe dissolved in the electrolyte solution. The R_{et} (Fig. 6c) of the (SiO_2 NPs)/GCE was larger than that of the bare electrode, showing that a layer of SiO_2 formed on the electrode surface could inhibit the electron transfer of the redox probe of $[Fe(CN)_6]^{3-/4-}$ to the electrode surface to some extent. whereas, the value of R_{et} (Fig. 6b) of the (SiO_2-P NPs)/GCE was much less than that of (SiO_2 NPs)/GCE (Fig. 6c) obviously and closed to that of bare GCE (Fig. 6a), indicating that SiO_2-P NPs had good conductivity and the (SiO_2-P NPs)/GCE could make the electron transfer easier between $[Fe(CN)_6]^{3-/4-}$ and the electrode surface.

The application of modified silica in electrochemistry mainly includes the following traits: Firstly, due to the large surface to volume ratio, nanoparticle agglomeration would happen, which may cause bad electrochemical performance. The surface modification of the particles can effectively prevent the reunion of nanoparticles [28,29]. And secondly, the conductivity is enhanced by the incorporation of modified silica and biomolecules [30]. Finally, single inorganic sol–gel thin film has its own inherent obstacles such as bad biocompatibility [31].

3.2. Direct electron transfer reactivity of the XOD/(SiO_2-P NPs)/GCE

Biological electrochemistry is a valuable and convenient tool to evaluate the biological protein activity and function. In order to investigate the electrochemical properties of XOD/(SiO_2-P NPs)/GCE, different modified electrodes were recorded by cyclic voltammogram (CV). Fig. 7 showed the CVs of different electrodes in 0.1 M PBS (pH 7.0) at a scan rate of 100 mV s^{-1}. The images showed CVs of bare GCE electrode (Fig. 7a), (SiO_2 NPs)/GCE electrode (Fig. 7b) and (SiO_2-P NPs)/GCE electrode (Fig. 7c) in the range of −1.0 to 0.2 V vs. SCE, in which no peak was observed as a result of the lack of redox-active biomoleculor XOD. After XOD was embedded in the (SiO_2-P NPs)/GCE (Fig. 7e), a pair of well-defined oxidation and reduction peaks could be observed, the anodic peak potential (E_{pa}) and cathodic peak potential (E_{pc}) were located at −0.35 and −0.38 V vs. SCE, respectively. However, for the XOD/(SiO_2 NPs)/GCE electrode (Fig. 7d), the observed oxidation–reduction peaks at the same place were lighter compared to that of on XOD/(SiO_2-P NPs)/GCE. These peaks resulted from direct electron transfer of the immobilized XOD attributed to the conversion of XOD (FAD)–XOD ($FADH_2$), which were consistent with values reported in the literatures for free FAD and the FAD redox center of the flavoenzyme [32,33]. Thus, the direct electrochemical reaction could be described as Eq. (3) [34]. The results of the CVs proved that SiO_2-P NPs must have a great effect on electrochemical response of the electrode reaction for XOD and provide a suitable microenvironment for the protein to transfer electrons with underlying GCE, that because the good biocompatibility of SiO_2-P NPs could provide the native microenvironment for XOD to orient in conformations more favorable for electron transfer.

3.3. Amperometric responses of XOD/(SiO_2-P NPs)/GCE to hypoxanthine

The amperometric response of the XOD/(SiO_2-P NPs)/GCE was investigated by successively adding different concentration of hypoxanthine in 0.1 M PBS (pH=7) solution under the optimized experimental condition (Fig. 8A). The XOD-catalyzed reactions taking place at the hypoxanthine biosensor had been illustrated in Eqs. (1) and (2) [18]. In the presence of molecular oxygen, XOD catalyzed the oxidation of hypoxanthine, upon addition of hypoxanthine to air-saturated PBS, a rapid increase in the anodic current appeared as a result of the oxidations of H_2O_2 and UA produced from the enzymatic reactions, which demonstrated that the biosensor based on SiO_2-P NPs exhibited a better electrocatalytic activity to hypoxanthine ascribed to their synergistic action of biocompatibility and conductivity. The experiments exhibited that the electrocatalytic response was very fast, because SiO_2-P NPs might provide a good micro-environment for XOD so that the redox system showed fast electrode kinetics. The corresponding calibration curve of current–time response of this biosensor was shown in Fig. 8B.

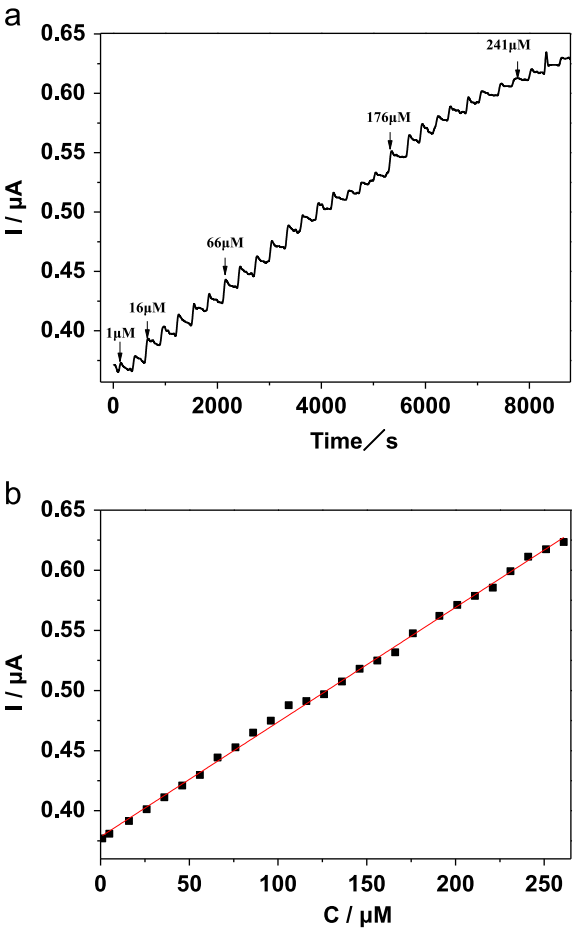

Fig. 8. (A) Typical current–time response of the XOD/(SiO_2-P NPs)/GCE on successive injection hypoxanthine into a stirred solution of 0.1 M phosphate buffer solution (pH 7.0) at applied potential 1.2 V. (B) Calibration curve of the biosensor.

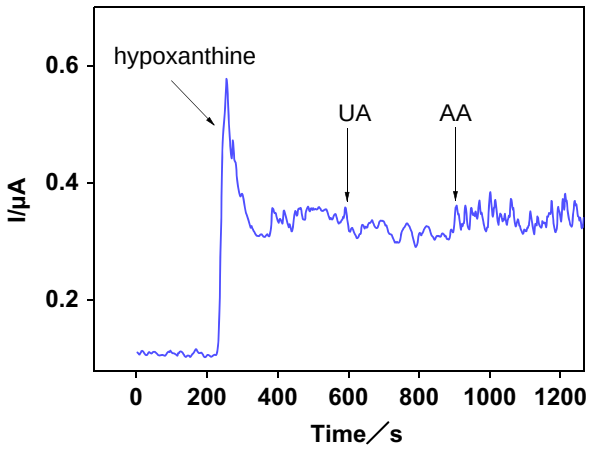

Fig. 9. Steady-state current–time responses of electrode to successive increments 20 μM hypoxanthine, 20 μM UA and 5 μM AA, respectively. Test condition: Eapp = 1.2 V, 0.1 M PBS (pH = 7.0).

Table 1
Comparison of the responses of some hypoxanthine biosensors based on different modified electrode materials.

Biosensor	Liner range (μM)	Detection limit (μM)	R-square	Ref.
GNPs–SWCNH/XOx	1.5–35.4	0.61	–	[35]
Nafion–XOx–Au	0.2–20	0.1	0.9994	[36]
(PCV)/MWCNTs–COOH	0.5–90	0.2	0.9985	[37]
XOD/HCPE	8.0–300	3.0	0.9960	[38]
XOD/CNT/CF	10–135	0.75	–	[39]
XOD/(SiO_2-P NPs)	1.0–261.0	0.23	0.9984	This work

After the addition of hypoxanthine, the anodic current immediately increased and reached 95% of steady state current within 5 s. The linear concentration range was from 1.00×10^{-6} to 2.61×10^{-4} M with a correlation coefficient of 0.9984. The detection limit of 2.33×10^{-7} M at a signal-to-noise ratio of 3 was lower than that most reported previously (Table.1) [35–39].

The repeatability of the biosensor was examined at the hypoxanthine concentrations of 10 mM, and the relative standard deviations for five determinations were less than 5% at five independently prepared biosensors, which indicated good reproducibility of the biosensor preparation. When the biosensor was stored in 0.1 M PBS with pH 7.0 at 4 °C, and used after two weeks, the enzyme electrode retained 88% of its initial activity. These results indicated acceptable stability.

$$\text{Hypoxanthine}+O_2\overset{\text{XOD}}{\Longrightarrow}\text{Xanthine}+H_2O_2 \quad (1)$$

$$\text{Xanthine}+O_2\overset{\text{XOD}}{\Longrightarrow}\text{Uric acid}+H_2O_2 \quad (2)$$

$$\text{XOD}-\text{FAD}+2e^-+2H^+\Longrightarrow\text{XOD}-\text{FADH}_2 \quad (3)$$

3.4. Anti-interference of XOD/(SiO_2-P NPs)/GCE biosensor

In real samples, some substances, for example, uric acid, ascorbic acid etc., may be the problems in the amperometric detection of analyte [18]. In order to investigate the selectivity and anti-interference advantages of the XOD/(SiO_2-P NPs)/GCE biosensor, some coexisting electroactive species were added to hypoxanthine solution. At the working potential, the amperometric responses at the XOD/(SiO_2-P NPs)/GCE electrode to the addition of hypoxanthine and two interfering substances (UA and AA) in 0.1 M PBS (pH 7.0) are shown in Fig. 9. The tested substances did not interfere significantly with the biosensor, no change in the response of the biosensor was found. The result was the same as that of without interferences. Hereby, we can conclude that the resulting biosensor has a strong anti-interference ability.

3.5. Fish samples analysis

The analytical reliability and application potential of the proposed biosensor was valuated for the determination of the concentration of hypoxanthine accumulated in fish continuously after death, which directly reflected the freshness of fish. Due to the lack of experimental conditions available to perform a traditional or referee determination, recovery testing was carried out to demonstrate the validity of the proposed method (Table 2).

After fish was killed and stored at room temperature for 0, 5, 12 and 24 h, the concentration of hypoxanthine increased from 6.15 to 7.34, 10.26 and 18.42 μM, respectively. The recoveries for the standard solutions of 10.0 μM are listed in Table 2. All of recoveries were from 93.34% to 96.11%, indicating acceptable accuracy. SiO_2-P NPs has a favorable electrical conductivity and SiO_2-P NPs provides a friendly microenvironment to retain XOD's bioactivity. The satisfying results demonstrated that the biosensor had a great potential for practical application.

Table 2
Determination of hypoxanthine content in fish samples using the XOD/(SiO_2-P NPs)/GCE biosensor.

Sample	Store condition	Added (μM) ± S.D[a]	Found(μM)	Recovery(%)
1	Fresh killed	6.15 ± 0.09	0	94.03
		15.18 ± 0.04	10	
2	5 h after death	7.34 ± 0.05	0	96.11
		16.71 ± 0.13	10	
3	12 h after death	10.26 ± 0.07	0	95.26
		19.30 ± 0.08	10	
4	24 h after death	18.42 ± 0.04	0	93.34
		26.51 ± 0.20	10	

[a] Mean value ± standard deviation (S.D.) of three measurements.

4. Conclusion

The phosphonic acid-functionalized silica nanoparticles had been successfully fabricated by the method of reverse microemulsion and electrostatic binding. Nanosized SiO_2-P NPs could provide a friendly microenvironment to retain XOD's bioactivity for the large amount of protein loading. The result of CD spectra indicated that near-native secondary structure of the protein on SiO_2-P NPs was retained. Immobilization of XOD on a surface of (SiO_2-P NPs)/GCE displayed good eletrocatalytical activity to hypoxanthine with a broad linear range from 1.00×10^{-6} to 2.61×10^{-4} M and a low detection of 2.33×10^{-7} M. In addition, the biosensor fabricated by XOD/(SiO_2-P NPs) on electrode also had a strong anti-interference ability in the presence of AA and UA. The biomimetic surface of SiO_2-P NPs played an important role to these super properties of the resulted biosensor, and could successfully detect hypoxanthine in fish samples as a great potential for practical application in electronic devices.

Acknowledgment

The work was supported by NSFC (20971069), NSFJS (BE2011196), the foundation of the Jiangsu education committee (CXZZ11_0890), Key Scientific and Technological Project of Shanghai Science and Technology Commission (10391901800), the Project Funded by the Priority Academic Program Development of Jiangsu Higher Education Institution, Base of PER of PJRP of Jiangsu (BY2011109), the Foundation of Jiangsu Collaborative Innovation Center of Biomedical Functional Materials, and the Natural Science Foundation of the Jiangsu Higher Education Institutions of China (11KJB150009).

References

[1] Y.Y. Zhang, S.Y. Deng, J.P. Lei, Q.N. Xu, H.X. Ju, Talanta 85 (2011) 2154–2158.
[2] Z.G. Chen, H.L. Chen, H. Hu, M.X. Yu, F.Y. Li, Q. Zhang, Z.G. Zhou, T. Yi, C.H. Huang, J. Am. Chem. Soc. 130 (2008) 3023–3029.
[3] L. Rassaei, M.J. Bonné, Mika. Sillanpää, F. Marken, New J. Chem. 32 (2008) 1253–1258.
[4] C. Sun, L.B. Chen, F.J. Xu, P.Y. Zhu, J.F. Luan, C. Mao, J. Shen, J. Mater. Chem. B 1 (2013) 801–809.
[5] G.F. Jie, L. Wang, J.X. Yuan, S.S. Zhang, Anal. Chem. 83 (2011) 3873–3880.
[6] W. Yan, X.M. Feng, X.J. Chen, W.H. Hou, J.J. Zhu, Biosens. Bioelectron. 23 (2008) 925–931.
[7] C. Sun, X.H. Chen, Q.R. Han, M. Zhou, C. Mao, Q.S. Zhu, J. Shen, Anal. Chim. Acta 776 (2013) 17–23.
[8] M. Shim, N.W. Kam, R.J. Chen, Y.M. Li, H.J. Dai, Nano Lett. 2 (2002) 285–288.
[9] V.B. Kandimalla, V.S. Tripathi, H. Ju, Crit. Rev. Anal. Chem. 36 (2006) 73–106.
[10] A. Collings, F. Caruso, Rep. Prog. Phys. 60 (1997) 1397–1445.
[11] J.J. Feng, Z.H. Li, Y.F. Li, A.J. Wang, P.P. Zhang, Microchim. Acta 176 (2012) 1–8.
[12] W.L. Zhu, Y. Wang, J. Xuan, J.R. Zhang, J. Nanosci. Nanotechnol. 11 (2011) 138–142.
[13] W.B. Zhao, Y. Fang, Q.S. Zhu, K. Wang, M. Liu, X.H. Huang, J. Shen, Electrochim. Acta 89 (2013) 278–283.
[14] W.B. Zhao, Y.L. Ni, Q.S. Zhu, R. Fu, X.H. Huang, J. Shen, Biosens. Bioelectron. 44 (2013) 1–5.
[15] R.R. Mendel, T. Kruse, BBA-Mol. Cell Res. 823 (2012) 1568–1579.
[16] B.S. Zuckerbraun, S. Shiva, E. Ifedigbo, M.A. Mathier, K.P. Mollen, J. Rao, P.M. Bauer, E. Curtis, M.T. Gladwin, B.S. Zuckerbraun, S. Shiva, E. Ifedigbo, M.A. Mathier, K.P. Mollen, J. Rao, P.M. Bauer, J.J. Choi, E. Curtis, A.M. Choi, M.T. Gladwin, Circulation 121 (2010) 98–109.
[17] M.A. Mir, J.M. Khan, R.H. Khan, A.A. Dar, G.M. Rather, J. Phys. Chem. B 116 (2012) 5711–5718.
[18] J. Zhang, J. Lei, R. Pan, Y. Xue, H. Ju, Biosens. Bioelectron. 26 (2010) 371–376.
[19] S.N. Ding, J.J. Xu, H.Y. Chen, Chem. Commun. 34 (2006) 3631–3633.
[20] R.P. Bagwe, L.R. Hilliard, W.H. Tan, Langmuir 22 (2006) 4357–4362.
[21] Discovery Studio, Version 2.1, Accelrys Inc., San Diego, CA, 2008.
[22] M.J. Frisch, G.W. Trucks, H.B. Schlegel, G.E. Scuseria, M.A. Robb, J.R. Cheeseman, J.A. Montgomery, T. Vreven, K.N. Kudin, J.C. Burant, J.M. Millam, S.S. Iyengar, J. Tomasi, V. Barone, B. Mennucci, M. Cossi, G. Scalmani, N. Rega, G.A. Petersson, H. Nakatsuji, M. Hada, M. Ehara, K. Toyota, R. Fukuda, J. Hasegawa, M. Ishida, T. Nakajima, Y. Honda, O. Kitao, H. Nakai, M. Klene, X. Li, J.E. Knox, H.P. Hratchian, J.B. Cross, C. Adamo, J. Jaramillo, R. Gomperts, R.E. Stratmann, O. Yazyev, A.J. Austin, R. Cammi, C. Pomelli, J.W. Ochterski, P.Y. Ayala, K. Morokuma, G.A. Voth, P. Salvador, J.J. Dannenberg, V.G. Zakrzewski, S. Dapprich, A.D. Daniels, M.C. Strain, O. Farkas, D.K. Malick, A.D. Rabuck, K. Raghavachari, J.B. Foresman, J.V. Ortiz, Q. Cui, A.G. Baboul, S. Clifford, J. Ioslowski, B.B. Stefanov, G. Liu, A. Liashenko, P. Piskorz, I. Komaromi, R.L. Martin, D.J. Fox, T. Keith, M.A. Al-Laham, C.Y. Peng, A. Nanayakkara, M. Challacombe, P.M.W. Gill, B. Johnson, W. Chen, M.W. Wong, C. Gonzalez, J.A. Pople, Gaussian 03, Revision B.05, Gaussian, Inc., Pittsburgh, PA, 2003.
[23] E. Hendry, T. Carpy, J. Johnston, M. Popland, R. Mikhaylovskiy, A. Lapthorn, S. Kelly, L. Barron, N. Gadegaard, M. Kadodwala, Nat. Nanotech. 5 (2010) 783–787.
[24] N. Sreerama, R.W. Woody, Method Enzymol. (2004) 318–351.
[25] X. Pang, P. Imin, I. Zhitomirsky, A. Adronov, Macromolecules 43 (2010) 10376–10381.
[26] P. Ye, Z.K. Xu, J. Wu, C. Innocent, P. Seta, Biomaterials 27 (2006) 4169–4176.
[27] K. Mequanint, A. Patel, D. Bezuidenhout, Biomacromolecules 7 (2006) 883–891.
[28] R.P. Bagwe, L.R. Hilliard, W. Tan, Langmuir 22 (2006) 4357–4362.
[29] S. Legrand, A. Catheline, L. Kind, E.C. Constable, C.E. Housecroft, L. Landmann, P. Banse, U. Pieles, A. Wirth-Heller, New J. Chem. 32 (2008) 588–593.
[30] Y. Zhao, Z. Jiang, D. Lin, A. Dong, Z. Li, H. Wu, J. Power Sour. 224 (2013) 28–36.
[31] W. Jin, J.D. Brennan, Anal. Chim. Acta 461 (2002) 1–36.
[32] C.G. Rodrigues, A.G. Wedd, J. Electroanal. Chem. 312 (1991) 131–140.
[33] L. Wang, Z. Yuan, Anal. Sci. 20 (2004) 635–638.
[34] D. Shan, Y.N. Wang, H.G. Xue, S. Cosnier, S.N. Ding, Biosens. Bioelectron. 24 (2009) 3556–3561.
[35] L. Zhang, J. Lei, J. Zhang, L. Ding, H. Ju, Analyst 137 (2012) 3126–3131.
[36] G.Y. Shi, M. Liu, M. Zhu, T.S. Zhou, J.S. Chen, L.T. Jin, J.Y. Jin, Analyst 127 (2002) 396–400.
[37] Y. Wang, Colloid Surf. B 88 (2011) 614–621.
[38] Z.Y. Lin, J.J. Sun, J.H. Chen, L. Guo, Y.T. Chen, G.N. Chen, Anal. Chem. 80 (2008) 2826–2831.
[39] A.C Torres, M.E Ghica, C.M.A Brett, Anal. Bioanal. Chem. 405 (2013) 3813–3822.